

# Hand-gesture recognition based on EMG and event-based camera sensor fusion: a benchmark in neuromorphic computing

Enea Ceolini<sup>1</sup>, Charlotte Frenkel<sup>1,2</sup>, Sumit Bam Shrestha<sup>3</sup>, Gemma Taverni<sup>1</sup>,  
Lyes Khacef<sup>4</sup>, Melika Payvand<sup>1</sup>, Elisa Donati<sup>1</sup>

<sup>1</sup>*Institute of Neuroinformatics, University of Zurich and ETH Zurich, Switzerland.*

<sup>2</sup>*ICTEAM Institute, Université catholique de Louvain, Belgium.*

<sup>3</sup>*Temasek Laboratories @ National University of Singapore, Singapore.*

<sup>4</sup>*Université Côte d'Azur, CNRS, LEAT, France.*

Correspondence\*:

Corresponding Author

elisa@ini.uzh.ch

## 2 ABSTRACT

3 Hand gestures are a form of non-verbal communication used by individuals in conjunction  
4 with speech to communicate. Nowadays, with the increasing use of technology, hand-gesture  
5 recognition is considered to be an important aspect of Human-Machine Interaction (HMI), allowing  
6 the machine to capture and interpret the user's intent and respond accordingly. The ability to  
7 discriminate human gestures can help in several applications such as assisted living, healthcare,  
8 neuro-rehabilitation, and sports. Recently, multi-sensor data fusion mechanisms have been  
9 investigated to improve discrimination accuracy. In this paper, we present a sensor fusion  
10 framework that integrates complementary systems: the electromyography (EMG) signal from  
11 muscles and visual information. This multi-sensor approach, while improving accuracy and  
12 robustness, introduces the disadvantage of high computational cost, which grows exponentially  
13 with the number of sensors and the number of measurements. Furthermore, this huge amount of  
14 data to process can affect the classification latency which can be crucial in real-case scenarios  
15 such as prosthetic control. Neuromorphic technologies can be deployed to overcome these  
16 limitations since they allow real-time processing in parallel at low power consumption. In this paper,  
17 we present a fully neuromorphic sensor fusion approach for hand-gesture recognition comprised  
18 of event-based vision sensor and three different neuromorphic processors. In particular, we used  
19 the event-based camera, called DVS, and two neuromorphic platforms, Loihi and ODIN+MorphIC.  
20 The EMG signals were recorded using traditional electrodes and then converted into spikes to

21 be fed into the chips. We collected a dataset of 5 gestures from sign language where visual  
22 and electromyography signals are synchronized. **We compared a fully neuromorphic approach**  
23 to a baseline implemented using traditional machine learning approaches on a portable GPU  
24 system. According to the chips constraints, we designed specific spiking neural networks (SNNs)  
25 for sensor fusion that showed classification accuracy comparable to the software baseline. These  
26 neuromorphic alternatives have increased **inference time**, between 20% and 40%, with respect  
27 to the GPU system but have a significantly smaller energy-delay product (EDP) which makes  
28 them between 30x and 600x more efficient. The proposed work represents a new benchmark  
29 that moves the neuromorphic computing towards a real-world scenario.

30 **Keywords:** Hand-gesture classification, Spiking Neural Networks (SNNs), Electromyography (EMG) Signal Processing, Event-based  
31 camera, Sensor Fusion, Neuromorphic Engineering

## 1 INTRODUCTION

32 Hand-gestures are considered a powerful communication channel for information transfer in daily life.  
33 Hand-gesture recognition is the process of classifying meaningful gestures of the hands, and is receiving  
34 renewed interest. The gestural interaction is a well-known technique that can be utilized in a vast array of  
35 applications (Yasen and Jusoh, 2019), such as sign language translation (Cheok et al., 2019), sports (Loss  
36 et al., 2012), Human-Robot Interaction (HRI) (Liu and Wang, 2018; Cicirelli et al., 2015), and more  
37 generally in Human-Machine Interaction (HMI) (Haria et al., 2017). Hand-gesture recognition systems also  
38 target medical applications, where they are detected via bioelectrical signals instead of vision. In particular,  
39 among the biomedical signals, electromyography (EMG) is the most used for hand-gesture identification  
40 and for the design of prosthetic hand controllers (Donati et al., 2019; Chen et al., 2020; Benatti et al., 2015).

41 EMG measures the electrical signal resulting from muscle activation. The source of the signal is the motor  
42 neuron action potentials generated during the muscle contraction. Generally, EMG can be detected either  
43 directly with electrodes inserted in the muscle tissue, or indirectly with surface electrodes positioned above  
44 the skin (surface EMG (sEMG)), for simplicity we will refer to it as EMG). The EMG is more popular  
45 for its accessibility and non-invasive nature. However, the use of EMG to discriminate hand-gestures is a  
46 non-trivial task due to several physiological processes in the skeletal muscles underlying their generation.

47 One way to overcome these limitations is to use a multimodal approach, combining EMG with recordings  
48 from other sensors. Multi-sensor data fusion is a direct consequence of the well-accepted paradigm that  
49 certain natural processes and phenomena are expressed under completely different physical guises (Lahat  
50 et al., 2015). In fact, multi-sensor systems provide higher accuracy by exploiting different sensors that  
51 measure the same signal in different but complementary ways. The higher accuracy is achieved thanks to a

52 redundancy gain that reduces the amount of uncertainty in the resulting information. Recent works show a  
53 growing interest toward multi-sensory fusion in several application areas such as developmental robotics  
54 (Droniou et al., 2015; Zahra and Navarro-Alarcon, 2019), audio-visual signal processing (Shivappa et al.,  
55 2010; Rivet et al., 2014), spatial perception (Pitti et al., 2012), attention-driven selection (Braun et al.,  
56 2019) and tracking (Zhao and Zeng, 2019), memory encoding (Tan et al., 2019), emotion recognition  
57 (Zhang et al., 2019), multi-sensory classification (Cholet et al., 2019), HMI (Turk, 2014), remote sensing  
58 and earth observation (Debes et al., 2014), medical diagnosis (Hoeks et al., 2011), and understanding brain  
59 functionality (Horwitz and Poeppel, 2002).

60 In this study we consider the complementary system comprising of a vision sensor and EMG  
61 measurements. Using EMG or camera systems separately presents some limitations, but their fusion  
62 has several advantages, in particular EMG-based classification can help in case of camera occlusion,  
63 whereas the vision classification provides an absolute measurement of hand state. This type of sensor fusion  
64 which combines vision and proprioceptive information is intensively used in biomedical applications, such  
65 as in transradial prosthetic domain to improve control performance (Markovic et al., 2014, 2015), or to  
66 focus on recognizing objects during grasping to adjust the movements (Došen et al., 2010). This last task  
67 can also use Convolutional Neural Networks (CNNs) as feature extractors (Ghazaei et al., 2017; Gigli et al.,  
68 2018).

69 While improving accuracy and robustness, the multiple input modalities also increase the computational  
70 cost, due to the amount of data to process in real-time that can affect the communication between the  
71 subject and the prosthetic hand. Neuromorphic technology offers a solution to overcome these limitations  
72 giving the possibility to process the multiple inputs in parallel in real-time, and with very low power  
73 consumption. Neuromorphic systems consist of circuits designed with principles based on the biological  
74 nervous systems that, similar to their biological counterparts, process information using energy-efficient,  
75 asynchronous, event-driven methods (Liu et al., 2014). These systems are often endowed with on-line  
76 learning abilities that allow adapting to different inputs and conditions. Lots of neuromorphic computing  
77 platforms have been developed in the past for modeling cortical circuits and their number is still growing  
78 (Merolla et al., 2014; Benjamin et al., 2014; Furber et al., 2014; Meier, 2015; Qiao et al., 2015; Moradi  
79 et al., 2017; Neckar et al., 2018; Davies et al., 2018; Frenkel et al., 2019a,b; Thakur et al., 2018).

80 In this paper we present a fully-neuromorphic implementation of sensor fusion for hand-gesture  
81 recognition. The proposed work is based on a previous work of sensor fusion for hand-gesture recognition,  
82 using standard machine learning approaches implemented in a mobile phone application for personalized  
83 medicine (Ceolini et al., 2019a). The paper showed how a CNN performed better, in terms of accuracy,  
84 than a Support Vector Machine (SVM) on the hand-gesture recognition task. The novelty introduced here

85 is that the sensor fusion is implemented on a fully neuromorphic system, from event-based camera sensor  
86 to the classification phase, performed by using three event-based neuromorphic circuits: Intel’s Loihi  
87 research processor (Davies et al., 2018) and a combination of the ODIN and MorphIC Spiking Neural  
88 Network (SNN) processors (Frenkel et al., 2019a,b). The two neuromorphic systems present different  
89 features, in particular, depending on the number of neurons available and on the input data, we implemented  
90 different SNN architectures. For example, for visual data processing, a spiking CNN is implemented in  
91 Loihi while a spiking Multi-Layer Perceptron (MLP) is chosen for ODIN + MorphIC, (see Section 2.3).  
92 For the case of EMG, the data was collected using the Myo armband that senses electrical activity in the  
93 forearm muscles. The data was later converted into spikes to be fed into the neuromorphic systems. Here,  
94 we propose a feasible application to show the neuromorphic performance in terms of accuracy, energy  
95 consumption and latency (**stimulus duration + inference time**). The performance metric for the energy  
96 consumption is the Energy-Delay Product (EDP), a metric suitable for most modern processor platforms  
97 defined as the average energy consumption multiplied by the average inference **time**. The inference **time**  
98 is defined as the time elapsed between the **end of** the stimulus and the classification. To validate the  
99 neuromorphic results, we are comparing to a baseline consisting of the network implemented using a  
100 standard machine learning approach where the inputs are fed as continuous EMG signals and video frames.  
101 We propose this comparison for a real case scenario as a benchmark, in order for the neuromorphic research  
102 field to advance into the mainstream of computing (Davies, 2019).

## 2 MATERIAL AND METHODS

103 In the following, we describe the overall system components. We start from the description of the sensors  
104 used to collect the hand-gesture data, namely the event-based camera, Dynamic Vision Sensor (DVS),  
105 and the EMG armband sensor, Myo. We then describe the procedure with which we collected the dataset  
106 used for the validation experiments presented here and that is publicly available. Afterwards, the two  
107 neuromorphic systems under consideration, namely Loihi and ODIN + MorphIC, will be described focusing  
108 on their system specifics, characteristics and the model architectures that will be implemented on them.  
109 Finally, we describe the system that we call baseline and that represents the point of comparison between a  
110 traditional von-Neumann approach and the two neuromorphic systems.

### 111 2.1 DVS and EMG Sensors

#### 112 2.1.1 DVS Sensor

113 The DVS (Lichtsteiner et al., 2006) is a neuromorphic camera inspired by the visual processing in the  
114 biological retina. Each pixel in the sensor array responds asynchronously to logarithmic changes in light.  
115 Whenever the incoming illumination increases or decreases above a certain threshold, it generates a polarity

116 spike event. The polarity corresponds to the sign of the change, ON polarity for increasing in light and  
117 OFF polarity for decreasing in light. The output is a continuous and sparse train of events interchangeably  
118 called spikes throughout this paper, carrying the information of the active pixels in the scene (represented  
119 in Figure 2). The static information is directly removed on the hardware side and only the dynamic one,  
120 corresponding to the movements in the scene, is actually transmitted. In this way the DVS can reach  
121 low latency, down to 10  $\mu$ s, reducing the power consumption needed for computation and the amount of  
122 transmitted data. Each spike is encoded using the Address Event Representation (AER) communication  
123 protocol (Deiss et al., 1999) and is represented by the address of the pixel (in x-y coordinates), the polarity  
124 (1 bit for the sign), and the timestamp (in microsecond resolution).

### 125 2.1.2 EMG Sensor

126 In the proposed work, we collected the EMG corresponding to the hand gestures by using the Myo  
127 armband by Thalmic Labs Inc. The Myo armband is a wearable device provided with eight equally spaced  
128 non-invasive EMG electrodes and a Bluetooth transmission module. The EMG electrodes detect the signals  
129 from the forearm muscles activity and afterwards the acquired data is sent to an external electronic device.  
130 The sampling rates for Myo data are fixed at 200Hz and the data is returned as a unitless 8-bit unsigned  
131 integer for each sensor representing ‘activation’ and does not translate to millivolts (mV).

## 132 2.2 DVS-EMG Dataset

133 The dataset is a collection of 5 hand gestures recorded with the two sensor modalities: muscle activity  
134 from the Myo and visual input, in form of DVS events. Moreover, the dataset also provides the video  
135 recording using a traditional frame-based camera, referred to as Active Pixel Sensor (APS) in the paper.  
136 The frames from the APS are used as ground truth and as input in the baseline models. The APS-frames  
137 provided in the dataset are gray-scale, 240x180 resolution. The dataset contains recordings from 21 subjects:  
138 12 males and 9 females of age from 25 to 35, (see Data Availability Statement for the full access to the  
139 dataset). The structure is the following: each subject repeats 3 sessions, in each session the subject performs  
140 5 hand gestures: *pinky*, *elle*, *yo*, *index* and *thumb* (see Figure 1), repeated 5 times. Each single gesture  
141 recording lasts 2s. The gestures are separated by a relaxing time of 1s, in order to remove any residual  
142 activity from the previous gesture. Every recording is cut in 10 chunks of 200ms each, this duration was  
143 selected to match the requirements of a real-case scenario of low latency prosthesis control where there  
144 is a need for the classification and creation of the motor command within 250 ms (Smith et al., 2011).  
145 Therefore, the final number of samples results to be 21(subjects) x 3(trials) x 5(repetitions) x 5(gestures) x  
146 10(chunks) for a total of 15750. The Myo records the superficial muscle activity at the middle forearm from  
147 8 electrodes with a sampling rate of 200Hz. During the recordings the DVS was mounted on a random  
148 moving system to generate relative movement between the sensor and the subject hand. The hand stands

149 static during the recording to avoid noise in the Myo sensor and the gestures are performed in front of a  
150 static white background, see Figure 1 for the full setup.

### 151 2.2.1 Implementation on neuromorphic devices

152 SNNs in general and their implementation on neuromorphic devices require inputs as spike trains. In the  
153 case of the DVS, the sensor output is already in form of spikes and polarity. The only requirement that  
154 we need to take into account is the limited number of neurons in the available neuromorphic processors.  
155 For this reason, we decided to crop the  $128 \times 128$  input of the DVS to  $40 \times 40$  centered on the hand-  
156 gesture. On the contrary, for the EMG, a conversion in the event-based domain is required. The solution  
157 used here is the delta-modulator ADC algorithm, based on a sigma-delta modulator circuit (Corradi  
158 and Indiveri, 2015). This mechanism is particularly used in low frequency, high performance and low  
159 power application (Lee et al., 2005) such as biomedical circuits. Moreover, this modulator represents a  
160 good interface for neuromorphic devices because it has much less circuit complexity and lower power  
161 consumption than multi-bit ADCs.

162 The delta-modulator algorithm transforms a continuous signal into two digital pulse outputs, UP or  
163 DOWN, according to the signal derivative. The UP (DOWN) spikes are generated every time the signal  
164 exceeds a positive (negative) threshold, like the ON (OFF) events from the DVS. As described before, the  
165 signal is sampled at 200Hz, this means that a new sample is acquired every 5 ms. To increase the time  
166 resolution of the generated spike train, which otherwise would contain too few spikes, the EMG signals are  
167 over-sampled to a higher frequency before undergoing the transformation into spikes (Donati et al., 2019).

168 For our specific EMG acquisition features, we set the threshold at 0.05 and an interpolation factor  
169 of 3500, these values have been selected from previous studies which looked at quality of signal  
170 reconstruction (Donati et al., 2018, 2019).

## 171 2.3 Neuromorphic processors

### 172 2.3.1 ODIN + MorphIC

173 The ODIN (Online-learning DIgital spiking Neuromorphic) processor occupies an area of only  $0.086\text{mm}^2$   
174 in 28nm FDSOI CMOS (Frenkel et al., 2019a)<sup>1</sup>. It consists of a single neurosynaptic core with 256 neurons  
175 and  $256^2$  synapses. Each neuron can be configured to phenomenologically reproduce the 20 Izhikevich  
176 behaviors of spiking neurons (Izhikevich, 2004). The synapses embed a 3-bit weight and a mapping table  
177 bit that allows enabling or disabling Spike-Dependent Synaptic Plasticity (SDSP) locally (Brader et al.,  
178 2007), thus allowing for the exploration of both off-chip training and on-chip online learning setups.

---

<sup>1</sup> The HDL source code and documentation of ODIN are publicly available at <https://github.com/ChFrenkel/ODIN>.



179 MorphIC is a quad-core digital neuromorphic processor with 2k LIF neurons and more than 2M synapses  
180 in 65nm CMOS (Frenkel et al., 2019b). MorphIC was designed for high-density large-scale integration  
181 of multi-chip setups. The four 512-neuron crossbar cores are connected with a hierarchical routing  
182 infrastructure that enables neuron fan-in and fan-out values of 1k and 2k, respectively. The synapses are  
183 binary and can be either programmed with offline-trained weights or trained online with a stochastic version  
184 of SDSP.

185 Both ODIN and MorphIC follow a standard synchronous digital implementation, which allows their  
186 operation to be predicted with one-to-one accuracy by custom Python-based chip simulators. As both chips  
187 rely on crossbar connectivity, CNN topologies can be explored but are limited to small networks due to an  
188 inefficient resource usage in the absence of a weight reuse mechanism (Frenkel et al., 2019b). The selected  
189 SNN architectures are thus based on fully-connected MLP topologies. Training is carried out in Keras  
190 with quantization-aware stochastic gradient descent following a standard ANN-to-SNN mapping approach  
191 (Hubara et al., 2017; Moons et al., 2017; Rueckauer et al., 2017), the resulting SNNs process the EMG and  
192 DVS spikes without further preprocessing.

193 In order to process the spike-based EMG gesture data, we selected ODIN so as to benefit from 3-  
194 bit weights. Indeed, due to the low input dimensionality of EMG data, satisfactory performance could  
195 not be reached with the binary weight resolution of MorphIC. A 3-bit-weight  $16-230-5$  SNN is thus  
196 implemented in ODIN, this setup will be referred to as the EMG-ODIN network.

197 For the DVS gesture data classification, we selected MorphIC in order to benefit from its higher neuron  
198 and synapse resources. **ON/OFF DVS events are treated equally and their connections to the network  
199 are learned, so that any of them can be either excitatory or inhibitory.** Similarly to a setup previously  
200 proposed for MNIST benchmarking (Frenkel et al., 2019b), the input  $40 \times 40$ -pixel DVS event streams  
201 can be subsampled into four  $20 \times 20$ -pixel event streams and processed independently in the four cores of  
202 MorphIC, thus leading to an accuracy boost when combining the outputs of all subnetworks, subsequently  
203 denoted as subMLPs. The four subMLPs have a  $400-210-5$  topology with binary weights, this setup  
204 will thus be referred to as the DVS-MorphIC network.

205 In order to ease sensor fusion, the hidden layer sizes of the EMG-ODIN and DVS-MorphIC networks and  
206 the associated firing thresholds were optimized by parameter search so as to balance their activities. These  
207 hidden layers were first flattened into a 1070-neuron layer, then a 5-neuron output layer was retrained with  
208 3-bit weights and implemented in ODIN. This setup will be referred to as the Fusion-ODIN network, which  
209 thus encapsulates EMG processing in ODIN, DVS processing in MorphIC and sensor fusion in ODIN.  
210 From an implementation point of view, mapping the MorphIC hidden layer output spikes back to ODIN for

211 sensor fusion requires an external mapping table. Its overhead is excluded from the results provided in  
212 Section 3.

### 213 2.3.2 Loihi and its training framework SLAYER

214 Intel’s Loihi (Davies et al., 2018) is an asynchronous neuromorphic research processor. Each Loihi chip  
215 consists of 128 neurocores, with each neurocore capable of implementing up to 1024 current based (CUBA)  
216 Leaky Integrate and Fire (LIF) neurons. The network state and configuration is stored entirely in on-chip  
217 SRAMs local to each core, this allows each core to access its local memories independently of other cores  
218 without needing to share a global memory bus (and in fact removing the need for off-chip memory). Loihi  
219 supports a number of different encodings for representing network connectivity, thus allowing the user to  
220 choose the most efficient encoding for their task. Each Loihi chip also contains three small synchronous  
221 x86 processors which help monitor and configure the network, as well as assisting with the injection of  
222 spikes and recording of output spikes.

223 SLAYER (Shrestha and Orchard, 2018) is a backpropagation framework for evaluating the gradient of  
224 any kind of SNN (i.e. spiking MLP and spiking CNN) directly in the spiking domain. It is a dt-based  
225 SNN backpropagation algorithm that keeps track of the internal membrane potential of the spiking neuron  
226 and uses it during gradient propagation. There are two main guiding principles of SLAYER: temporal  
227 credit assignment policy and probabilistic spiking neuron behavior during error backpropagation. Temporal  
228 credit assignment policy acknowledges the temporal nature of a spiking neuron where a spike event at a  
229 particular time has its effect on future events. Therefore, the error credit of an error at a particular time  
230 needs to be distributed back in time. SLAYER is one of the few methods that consider temporal effects  
231 during backpropagation. The use of probabilistic neurons during backpropagation helps estimate the spike  
232 function derivative, which is a major challenge for SNN backpropagation, with the spike escape rate  
233 function of a probabilistic neuron. The end effect is that the spike escape rate function is used to estimate  
234 the spike function derivative, similar to the surrogate gradient concept (Zenke and Ganguli, 2018; Neftci  
235 et al., 2019). With SLAYER, we can train synaptic weights as well as axonal delays and achieve state of  
236 the art performances (Shrestha and Orchard, 2018) on neuromorphic datasets.

237 SLAYER uses the versatile Spike Response Model (SRM) (Gerstner, 1995) which can be customized  
238 to represent a wide variety of spiking neurons with a simple change of spike response kernels. It is  
239 implemented<sup>2</sup> atop the PyTorch framework with automatic differentiation support (Paszke et al., 2017)  
240 with the flexibility of feedforward dense, convolutional, pooling and skip connections in the network.

---

<sup>2</sup> SLAYER-PyTorch is publicly available at <https://github.com/bamsumit/slayerPytorch>.



SLAYER-PyTorch also supports training with the exact CUBA Leaky Integrate and Fire neuron model in Loihi (Davies et al., 2018). To train for the fixed precision constraints on weights and delays of Loihi hardware, it trains the network with the quantization constraints and then trains using the strategy of shadow variables (Courbariaux et al., 2015; Hubara et al., 2016) where the constrained network is used in forward propagation phase and the full precision shadow variables are used during backpropagation.

We used SLAYER-PyTorch to train a Loihi compatible network for the hand-gesture recognition task. The networks were trained offline using GPU and trained weights and delays were used to configure the network on Loihi hardware for inference purposes. All the figures reported here are for inference using Loihi with one algorithmic time tick in Loihi of 1 *ms*.

A spiking MLP of architecture 16-128d-128d-5 was trained for EMG gestures converted into spikes (Section 2.2.1). Here, 128d means the fully connected layer has 128 neurons with trained axonal delays. The Loihi neuron with current and voltage decay constants of 1024 (32 ms) was used for this network.

For the gesture classification using DVS data we used both a spiking MLP, with the same architecture as the one deployed on MorphIC and described in Section 2.3.1, and a spiking CNN with architecture 40×40×2-8c3-2p-16c3-2p-32c3-512-5. Here, XcY denotes a convolution layer with X kernels of shape Y-by-Y, while 2p denotes a 2-by-2 max pooling layer. Zero padding was applied for all convolution layers. No preprocessing on the spike events was performed, **the ON/OFF events are treated as different input channels, hence the input shape 40×40×2**. For this network, current and voltage decay constants for the Loihi neurons were set to 1024 (32 ms) and 128 (4 ms).

Finally, a third network where the penultimate layer neurons of DVS and EMG networks were fused together was trained. Only the last fully connected weights (640-5) were trained. The parameters of the network before fusion were preserved. The current and voltage decay constants of 1024 (32 ms) and 128 (4 ms) respectively were used for the final fusion layer neurons. From now on, we will refer these three networks as EMG-Loihi, DVS-Loihi, and Fusion-Loihi whenever there is ambiguity.

## 2.4 Traditional machine learning baselines

Machine Learning (ML) methods, and in general data-driven approaches, are currently the dominant tools to solve complex classification tasks since they give the best performance compared to other approaches. We compare the performance of the two fully neuromorphic systems described in the above sections, against a traditional machine learning pipeline that uses frame-based inputs, i.e. traditionally sampled EMG signals and traditionally sampled video frames. In order for the comparisons to be fair, for the traditional approach we maintain the same constraints imposed by the neuromorphic hardware. In particular, we used the same neural network architectures as those used in the neuromorphic systems. Note that **two**

273 different networks were implemented, spiking MLP and spiking CNN (see Figure 3 for more details on the  
 274 architectures). For this reason, we have two different baseline models that are paired to the two considered  
 275 neuromorphic systems.

#### 276 2.4.1 EMG Feature extraction

277 Traditional EMG signal processing consists of various steps. First, signal pre-processing is used to extract  
 278 useful information by applying filters and transformations. Then, feature extraction is used to highlight  
 279 meaningful structures and patterns. Finally, a classifier maps the selected features to output classes. In  
 280 this section we describe the EMG feature extraction phase, in particular we consider time domain features  
 281 used for the classification of gestures with the baseline models. We extracted two time domain features  
 282 generally used in literature (Phinyomark et al., 2018), namely Mean Absolute Value (MAV) and Root  
 283 Mean Square (RMS) shown in Equations 1. The MAV is the average of the muscles activation value and it  
 284 is calculated by a stride-moving window. The RMS is represented as amplitude relating to a gestural force  
 285 and muscular contraction. The two features are calculated across a window of 40 samples, corresponding  
 286 to 200 ms:

$$MAV(x_c) = \frac{1}{T} \sum_{t=0}^T |x_c(t)| \quad RMS(x_c) = \sqrt{\frac{1}{T} \sum_{t=0}^T x_c^2(t)} \quad (1)$$

where  $x_c(t)$  is the signal in the time domain for the EMG channel with index  $c$  and  $T$  is the number of  
 samples in the considered window, which was set to be  $T = 40$  ( $N = 200$  ms) across this work. The  
 features were calculated for each channel separately and the resulting values were concatenated in a vector  
 $\mathbf{F}(n)$  described in Equation 2:

$$\mathbf{F}(n) = [F(x_1), \dots, F(x_C)]^T \quad (2)$$

287 where  $\mathbf{F}$  is MAV or RMS,  $n$  is the index of the window and  $C$  is the number of EMG channels. The final  
 288 feature vector  $\mathbf{E}(n)$  for window  $n$  is shown in Equation 3, it is used for the classification and is obtained by  
 289 concatenating the two single feature vectors

$$\mathbf{E}(n) = [\mathbf{MAV}(n)^T, \mathbf{RMS}(n)^T]^T \quad (3)$$

#### 290 2.4.2 Baseline ODIN + MorphIC

291 As described in Section 2.3.1, a CNN cannot be efficiently implemented on crossbar cores, which is the  
 292 architecture ODIN and MorphIC rely on. We will therefore rely solely on fully-connected MLPs networks  
 293 for both visual and EMG data processing. For the visual input, we used the same subMLP-based network

294 structure as the one described in Section 2.3.1, but with gray-scale APS frames. The 40x40 cropped APS  
295 frames are sub-sampled and fed into four 2-layer subMLPs of architecture 400–210–5, as shown in  
296 Figure 3 panel (b). The outputs of the 4 subMLPs are then summed when classifying with a single sensor  
297 and are concatenated for the fusion network. The EMG neural network is a 2-layer MLP of architecture  
298 16–230–5. The fusion network is obtained as described above for the Loihi baseline.

### 299 2.4.3 Baseline Loihi

300 As described in Section 2.3.2, we used a spiking MLP and a spiking CNN to process and classify DVS  
301 events. For the Loihi baseline, we kept the exact same architectures, except for the axonal delays. Moreover,  
302 both architectures of the baseline receive the corresponding gray-scale APS frames instead of the DVS  
303 events. The baseline MLP architecture and the CNN architectures are shown in Figure 3 panel (a) and (b)  
304 respectively. Note that the number of parameters between the baseline networks and the spiking networks  
305 implemented on Loihi is slightly different since the input has 1 channel (gray-scale) in the case of the  
306 baseline that uses APS frames while it has 2 channels (polarity) in the input for Loihi.

307 The MLP architecture used for the EMG classification is instead composed of 2 layers of 128 followed  
308 by one layer of 5 units. While the input stays of the same size (16) with respect to the network implemented  
309 on Loihi, the input features are different since the baseline MLP receives MAV and RMS features while  
310 the Loihi receives spikes obtained from the raw signal.

311 To obtain the fusion network, we eliminate the last layer (classification layer) from both the single  
312 sensor networks, concatenate the two penultimate layers of the single sensor networks and add a common  
313 classification layer with 5 units, one per each class.

### 314 2.4.4 Training and Deployment

315 The models are trained with Keras using Adam optimizer with standard parameters. First, the single  
316 modality networks are trained separately, each for 30 epochs. For sensor fusion, output layer retraining  
317 is also carried out for 30 epochs. In order to compare the baselines against the neuromorphic systems  
318 in terms of energy consumption and inference time, we deployed the baseline models onto the NVIDIA  
319 Jetson Nano, an embedded system with a 128-Core Maxwell GPU with 4GB 64-bit LPDDR4 memory  
320 25.6 GB/s<sup>3</sup>.

## 3 RESULTS

321 Table 1 summarizes the results for Loihi and ODIN+MorphIC with the respective baselines. More details  
322 are described in the following sections.

---

<sup>3</sup> <https://developer.nvidia.com/embedded/jetson-nano-developer-kit>

### 3.1 Loihi results

The classification performances of these three networks, EMG-Loihi, DVS-Loihi, and Fusion-Loihi, with three-fold cross-validation and inferenced using 200 ms data are tabulated in Table 2. The core utilization, dynamic power consumption and inference time in the Loihi hardware are also listed in Table 2. The dynamic power is measured as the difference of total power consumed by the network and the static power when the chip is idle. Since one algorithmic time tick is 1ms long, inference time represents the speedup factor compared to real time.

With the spiking MLP implemented on Loihi, we obtained an accuracy of  $50.3 \pm 1.5\%$ ,  $83.1 \pm 3.4\%$  and  $83.4 \pm 2.1\%$  for the hand-gesture classification task using EMG, DVS and fusion respectively. Being that these results were significantly worse than the ones obtained with the spiking CNN, we do not report them in Table 1 and Table 2 and prefer to focus our analysis on the CNN which is better suited for visual tasks. This poor performance is due to temporal resolution of Loihi that causes a drop in the number of spikes in the MLP architecture while this does not happen in the CNN architecture.

The EMG network does not perform as well as in the baseline as shown in Table 1. The reason for this discrepancy can be found in the fact that the baseline method uses EMG from the raw signal of the sensor. However, to process this signal using neuromorphic chips (Loihi and ODIN+MorphIC), the EMG signal is encoded into spikes. With this encoding, part of the information is lost (as is the case for any encoding). Therefore, the baseline method has the advantage of using a signal that has more information and thus it outperforms the neuromorphic approach. Note that these Loihi networks are restricted to 8-bit fixed precision weights and 6-bit fixed precision delays.

To evaluate the performance **over time** of the Loihi networks, **stimulus duration** versus testing accuracy is plotted in Figure 4. We can see that the EMG-Loihi network continues to improve with longer **stimulus duration**. Table 1 and Figure 4 show the results of the Loihi baseline. From an accuracy point of view the baseline reaches a higher classification accuracy only in the EMG classification, while both the visual classification and fusion are on par with the Loihi networks and show only a non-significant difference. In terms of inference time, the baseline running on the GPU system is systematically faster than Loihi, but never more than 40% faster. As expected, the energy consumption of the GPU system is significantly higher than the Loihi system. Loihi is around 30x more efficient than the baseline for what concerns the fusion network and more than 150x and 40x more efficient for what concerns the EMG and DVS processing respectively. Figure 4 shows in more details the effect of **stimulus duration** on the classification accuracy. As expected, EMG is the modality that suffers more from classification based on short segments (Smith et al., 2011), reaching for both the neuromorphic system and the baseline the best accuracy only after 200 ms, while the accuracy for vision and fusion modalities saturate much more quickly, in around 100 ms for the

356 neuromorphic system and 50 ms for the baseline. The traditional system reaches its best performance after  
 357 50 ms while the neuromorphic system reaches its best performance after 200ms. One should, however, also  
 358 note that the DVS sensor contains only the edge information of the scene whereas the baseline network  
 359 uses the image frame. Therefore, the spiking CNN requires some time to integrate the input information  
 360 from DVS. Despite the inherent delays in a spiking CNN, the Loihi CNN can respond to the input within a  
 361 few ms of inputs. However, for the vision modality, notice that, because the frame rate of the camera is 20  
 362 fps, there is no classification before 25ms. Therefore, for **short stimulus duration**, the neuromorphic system  
 363 **has higher accuracy** than the traditional system.

### 364 3.2 ODIN + MorphIC results

365 Inference statistics for a 200 ms sample duration are reported in Table 3 for the EMG-ODIN, DVS-  
 366 MorphIC and Fusion-ODIN networks. Chip utilization is computed as the percentage of neuron resources  
 367 taken by the hidden and output layers in ODIN and MorphIC, while the power consumption  $P$  of the  
 368 crossbar cores of both chips can be decomposed as

$$P = P_{\text{leak}} + P_{\text{idle}}f_{\text{clk}} + E_{\text{SOP}}r_{\text{SOP}}, \quad (4)$$

369 where  $P_{\text{leak}}$  is the chip leakage power and  $P_{\text{leak}} + P_{\text{idle}}f_{\text{clk}}$  represents the static power consumption when  
 370 a clock of frequency  $f_{\text{clk}}$  is connected, without network activity. The term  $E_{\text{SOP}}r_{\text{SOP}}$  thus represents the  
 371 dynamic power consumption, where  $E_{\text{SOP}}$  is the energy per synaptic operation (SOP) and  $r_{\text{SOP}}$  is the  
 372 SOP processing rate, each SOP taking two clock cycles. Detailed power models extracted from chip  
 373 measurements of ODIN and MorphIC are provided in (Frenkel et al., 2019a) and (Frenkel et al., 2019b),  
 374 respectively. The results reported in Tables 1 and 3 are obtained with ODIN and MorphIC optimizing for  
 375 power, under the conditions summarized in Table 4. The dynamic power consumption reported in Table 4  
 376 reflects the regime in which ODIN and the four cores of MorphIC run at the maximum SOP processing  
 377 rate  $r_{\text{SOP}} = f_{\text{clk}}/2$ .

378 A limitation of the crossbar-based architecture of ODIN and MorphIC is that each neuron spike leads to a  
 379 systematic processing of all neurons in the core, thus potentially leading to a significant amount of dummy  
 380 operations (Frenkel et al., 2019b). Taking the example of the DVS-MorphIC network with a crossbar core  
 381 of 512 neurons (Figure 3, panel (b)), each input spike leads to 512 SOPs, of which only 210 are useful for  
 382 hidden layer processing. Similarly, each spike from a hidden layer neuron leads to 512 SOPs, of which  
 383 only 5 are actually used for output layer processing. The induced overhead is thus particularly critical for  
 384 output layer processing, which degrades both the energy per inference and the inference time.<sup>4</sup> However,

<sup>4</sup> As discussed in (Frenkel et al., 2019b), a simple extension providing post-synaptic start and end addresses would avoid these dummy SOPs and allow for an efficient processing of fully-connected layers, which will be included in future generations of the chips.

385 this problem is partly mitigated in the Fusion-ODIN network for output layer processing. Indeed, when  
386 resorting to an external mapping table (Section 2.3.1), hidden layer spikes can be remapped back to the  
387 sensor fusion output layer of ODIN with specific single-SOP AER events (Frenkel et al., 2019a), thus  
388 avoiding the dummy SOP overhead and leading to a lower energy and inference time compared to the  
389 standalone EMG-ODIN and DVS-MorphIC networks (Tables 1 and 3). As described in Section 2.3.1, the  
390 fusion results exclude the mapping table overhead.

391 The comparison of the results obtained with ODIN + MorphIC to those obtained with its GPU baseline  
392 counterpart (Table 1 and Figure 5) leads to conclusions similar to those already drawn with Loihi in  
393 Section 3.1, with the difference that while the GPU system is significantly faster, between 2x to 10x  
394 faster, the ODIN + MorphIC neuromorphic system is between **500× and 3200×** more energy-efficient.  
395 Moreover, it appears from Figure 5 that the EMG-ODIN, DVS-MorphIC and Fusion-ODIN networks  
396 basically perform at chance level for a 10-ms **stimulus duration**. This comes from the fact that the firing  
397 thresholds of the networks were selected based on a 200-ms **stimulus duration**, which leads the output  
398 neurons to remain silent and never cross their firing threshold when insufficient input spike data is provided.  
399 This problem could be alleviated by reducing the neuron firing thresholds for shorter **stimulus durations**.

### 400 **3.3 EDP and computational complexity**

401 Figure 6 shows a comparison between the Loihi system and the ODIN + MorphIC system in terms of EDP,  
402 number of operations per classification and a ratio between these two quantities. While panel (a) reports the  
403 same numbers as in Table 1, panels (b) and (c), allow for a more fair comparison of energy consumption  
404 between the two neuromorphic systems. From panel (b), we can see how the number of operations is similar  
405 for the EMG networks, being both MLPs for the two neuromorphic systems. Differently, the numbers of  
406 operations for the visual input and the fusion differ substantially between the two systems due to the use of  
407 a CNN in the Loihi system. Taking this into account, we can see in panel (c) that the normalized energy  
408 consumption tends to be similar for both systems more than the EDP in panel (a) is.

## 4 **DISCUSSIONS**

409 As it has been discussed in (Davies, 2019), there is a real need for a benchmark in the neuromorphic  
410 engineering field to compare the metrics of accuracy, energy, and latency. ML benchmarks such as ImageNet  
411 for image classification (Deng et al., 2009), Chime challenges for speech recognition (Barker et al., 2015)  
412 and Ninapro dataset containing kinematic and surface EMG for prosthetic applications (Atzori et al., 2014)  
413 are not ideal for neuromorphic chips as they require high performance computing for processing. For  
414 example, floating point bit resolution, large amounts of data and large power consumption. There have  
415 been some efforts in creating relevant event-based datasets such as N-MNIST (Orchard et al., 2015), the



416 spiking version of the widespread MNIST digits recognition dataset, N-TIDIGITS18 (Anumula et al.,  
417 2018), the spiking version of the spoken digits recognition dataset from LDC TIDIGITS, and DVS gesture  
418 recognition dataset from IBM (Amir et al., 2017). These datasets are either toy examples, or are not meant  
419 for real-world applications. Here, we are introducing a hand gesture benchmark in English sign language  
420 (e.g. ILY) using the DVS and Myo sensors. This kind of benchmark can be directly used as a preliminary  
421 test for Brain-Machine Interface (BMI)/personalized medicine applications. We have collected this dataset  
422 from 21 people and in this paper have benchmarked it on three digital neuromorphic chips, measuring the  
423 accuracy, energy and **inference time**. We believe this work takes an important first step in the direction of  
424 a real use-case (e.g. rehabilitation, sports applications, and sign interpretation) which we would like to  
425 encourage the community to use.

426 Although the dataset we provided is on static gestures, the DVS and the spiking EMG signals provide the  
427 capability for low-power processing using event-based neuromorphic chips and enable embedded systems  
428 with online on-site processing without having to send the data to remote sensors. Therefore, this work is an  
429 important first step towards edge-computing applications. The static dataset also helps with reducing the  
430 noise from the EMG signals as we mentioned in Section 2.2. However, this does not move away from the  
431 real application as we have shown in a live demo in (Ceolini et al., 2019).

432 The selected multi-sensor data fusion, that combines vision and EMG sensors, derives from the need  
433 of multiple sources to help the classification in real-scenario cases. Although the results show a small  
434 improvement due to the EMG sensors, they still **provide some** classification in case of not ideal light  
435 conditions or camera occlusions. In addition, for specific applications such as neuroprosthetic control, the  
436 EMG is integrated in the prosthetic device and, eventually, the camera can act as support input helping  
437 during calibration or more advanced tasks, such as sensory-motor closed loop (Jiang et al., 2012).

438 Since the event-based neuromorphic chips require inputs in the form of events, the continuous sensory  
439 signals have to be encoded into spikes for an event-driven processing. This quantization loses information  
440 (and hence accuracy) in comparison to the analog information processing in trade-off with the low power  
441 consumption of event-based systems which is required for edge computing. To compensate for the loss  
442 of information and accuracy, it is important to merge information from multiple sensors in a sensory  
443 fusion setup. In this setting, the information loss by quantization from one sensor can be made up for by  
444 another one. This is similar to how humans and animals perceive their environment through diverse sensory  
445 channels: vision, audition, touch, smell, proprioception, etc. From a biological perspective, the fundamental  
446 reason lies in the concept of degeneracy in neural structures (Edelman, 1987), which means that any single  
447 function can be carried out by more than one configuration of neural signals, so that the biological system  
448 still functions with the loss of one component. It also means that sensory systems can educate each other,

449 without an external teacher (Smith and Gasser, 2005). The same principles can be applied for artificial  
450 systems, as information about the same phenomenon in the environment can be acquired from various  
451 types of sensors: cameras, microphones, accelerometers, etc. Each sensory-information can be considered  
452 as a modality. Due to the rich characteristics of natural phenomena, it is rare that a single modality provides  
453 a complete representation of the phenomenon of interest (Lahat et al., 2015).

454 There are mainly two strategies for multi-modal fusion in the literature (Cholet et al., 2019): (1) data-level  
455 fusion (early fusion) where modalities are concatenated then learned by a unique model, and (2) score-level  
456 fusion (late fusion) where modalities are learned by distinct models and only after their predictions are  
457 fused with another model that provides a final decision. Early fusion, including feature-level fusion, suffers  
458 from a compatibility problem (Peng et al., 2016) and does not generalize well. Additionally, neural-based  
459 early fusion increases the memory footprint and the computational cost of the process, by inducing a full  
460 connectivity at the first classification stages. It is an important factor to take in consideration when choosing  
461 a fusion strategy (Castanedo, 2013), especially for embedded systems. Therefore, we follow a late fusion  
462 approach with a classifier-level fusion, that has been shown to perform better than feature-level fusion  
463 for classification tasks (Guo et al., 2014; Peng et al., 2016; Biagetti et al., 2018). It is close to score-level  
464 fusion by combining the penultimate layers of the base (unimodal) classifiers in a meta-level (multimodal)  
465 classifier that uses the natural complementarity of different modalities to improve the overall classification  
466 accuracy.

467 In this context, to have a fair comparison, the central question is the difference between the completely  
468 traditional approaches, such as the CNN and MLP baselines, versus the event-based neuromorphic one.  
469 In the baseline, the EMG features are manually extracted and the classification is done on the extracted  
470 features. Note that this pipeline is completely different from the event-based neuromorphic approach which  
471 extracts the features directly from the events. Another important thing to mention here is that although  
472 we have encoded the signals separately, this sensory information can be directly encoded to events at  
473 the front-end. This has already been established for audio and visual sensors (Lichtsteiner et al., 2006;  
474 Chan et al., 2007) and there have also recently been design efforts for other signals such the biomedical  
475 ones (Corradi and Indiveri, 2015).

476 To have a reference point for comparison, we trained the same network architecture used for the two  
477 neuromorphic setups. As it can be seen in Table 1, the baseline accuracy on the fusion is on par with both  
478 Loihi and ODIN+MorphIC, despite the lower bit resolution on the neuromorphic chips in comparison with  
479 the 32-bit floating point resolutions on GPU in the baseline approach. We speculate this is because the  
480 SLAYER training model already takes into account the low bit precision and thus calculates the gradients  
481 respectively. Similar to that, ODIN and MorphIC take a quantization-aware training approach which

calculates the weights based on the available on-chip precision. As can be seen from all the experiments in Table 1, the classification accuracy using only the EMG sensor is relatively low. However, it is to be noticed that this is a result of having a model which is trained across subjects and there are multiple sources of variability across subjects: i) The placement of the EMG sensor is not necessarily in the same position (with respect to the forearm muscles) for every subject. ii) Every subject performs the gestures in a unique manner iii) The muscle strength is different for every subject. In addition, since the EMG is directly measured from surface electrodes, it acquires noise while traveling through the skin, background noise from electronics, ambient noise, and so forth. In a real-world application, the network model can be trained on a single subject's data yielding much higher accuracy. Moreover, having the online learning abilities on the neuromorphic chip can aid in adapting these models to every subject uniquely. Such online learning modules are already existent in Loihi as well as in ODIN and MorphIC, which can be exploited in the future for boosting the classification accuracy of EMG signals. Also, it becomes apparent that the fusion accuracy is close, even if higher of about 4%, to the accuracy achieved with the DVS single sensor. However, the importance of the EMG signal is in the wearable application since it is a natural way to control prosthesis and it is a direct measure of the activity and movement in the muscles. Given the noisy nature of the EMG signal, it is critical to combine it with the visual input to boost the accuracy. But even given the noisy nature of the signal, it still allows to retrieve relevant information which helps boosting the accuracy of the fusion.

It is worth noting that while the accuracy between the spiking MLP on Loihi and ODIN+MorphIC are directly comparable, the results regarding the spiking CNN on Loihi and the spiking MLP on ODIN+MorphIC are not. This is because the two architectures use different features and resources on their respective neuromorphic systems (as already described in Section 2.3). Based on this, there are different constraints present in the two chips. Traditionally, a CNN architecture is used for image classification which is the network we used on the Loihi chip given the large number of neurons that are available (128k) on this general purpose platform. However, since ODIN and MorphIC are small-scale devices compared to Loihi, the number of neurons are a lot more constrained (i.e. 256 neurons for ODIN, 2k for MorphIC). Therefore, we resorted to using a fully-connected MLP topology instead of a CNN for image classification in MorphIC.

Regarding the latency, it is important to mention that for real-world prosthetic applications, the latency budget is below 250 ms (Smith et al., 2011). This means that if the processing happens within this budget, the patient will not feel the lag of the system. Hence, optimizing the system for having lower latency than 200 ms will not be beneficial as the patient will not feel the latency below 200 ms. Therefore, within this budget, other parameters can be optimized. The neuromorphic approach is very advantageous in this case

515 since it trades-off power with latency but it stays within the latency budget that is required. Contrarily,  
516 the GPU system has an overall faster inference time but uses much more energy. It is worth mentioning  
517 that our results are reported in accelerated time, however, the EMG and DVS are slowly changing signals  
518 and thus even though the classification is done very fast, the system has to wait for the inputs to arrive.  
519 Therefore, it is as if the system is being run in real-time. Here, there is a trade-off between the memory that  
520 is storing the streaming data for processing and the dynamic energy consumption. The accelerated time  
521 allows the lower energy consumption as the system is on for a shorter time, however, this comes with the  
522 caveat that the input has to be buffered for at least 200 ms in off-chip memory, therefore inducing a power  
523 and resource overhead.

524 The final comparison provided by Figure 6 shows how the two systems have a similar energy consumption  
525 when this is normalized by the number of operations done to run the network and obtain one classification  
526 output. While ODIN + MorphIC consumes less per classification in absolute terms, when considering  
527 the number of operations, it performs comparably to Loihi. When deploying a neuromorphic system one  
528 has to take into account all these aspects. Meaning not only there is a trade-off between speed and energy  
529 consumption but there is also one between accuracy and energy consumption given the fact that a more  
530 complex network architecture may have more predictive power while coming with a higher energy demand.  
531 Overall, one has to look for the best trade-off in the context of a particular application, the malleability of  
532 neuromorphic hardware enables this adaptation to the task-dependent constraints within a framework of  
533 state of the art results with respect to system performance.

## CONFLICT OF INTEREST STATEMENT

534 The authors declare that the research was conducted in the absence of any commercial or financial  
535 relationships that could be construed as a potential conflict of interest.

## AUTHOR CONTRIBUTIONS

536 EC, CF, SBS contributed equally to the work. EC, GT, MP, ED participate equally to the development of  
537 the work idea and collected the dataset. EC, LK were responsible for the baselines experiments. CF and  
538 SBS implemented the ODIN+MorphIC and Loihi pipelines respectively. SBS implemented the SLAYER  
539 framework and adapted it for the specific application. Everyone contributed to the writing of the paper.

## FUNDING

540 This work is supported by the EU's H2020 MSC-IF grant NEPSpiNN (Grant No. 753470), the Swiss  
541 Forschungskredit grant FK-18-103, the Toshiba Corporation, the Swiss Forschungskredit grant FK-19-106,

542 the SNSF grant No. 200021.172553 the fonds européen de développement régional FEDER, the Wallonia  
543 within the “Wallonie-2020.EU” program, the Plan Marshall, the FRS-FNRS of Belgium, and the H2020  
544 MC SWITCHBOARD ETN (Grant No. 674901).

545 The authors declare that this study received funding from Toshiba Corporation. The funder was not  
546 involved in the study design, collection, analysis, interpretation of data, the writing of this article or the  
547 decision to submit it for publication.

## ACKNOWLEDGMENTS

548 The authors would like to acknowledge the 2019 Capocaccia and Telluride Neuromorphic Workshops  
549 and all their participants for the fruitful discussions, Intel Corporation for access to Loihi neuromorphic  
550 platform. We thank Prof. B. Miramond, Prof. D. Bol, Prof. S. Liu, Prof. T. Delbruck and Prof. G. Indiveri.  
551 Finally, we thank Garrick Orchard for supporting us with the use of the Loihi platform and the useful  
552 comments to the paper.

## DATA AVAILABILITY STATEMENT

553 The datasets analyzed for this study can be found in the Zenodo, open access repository (Ceolini  
554 et al., 2019b), <http://doi.org/10.5281/zenodo.3663616>. Ceolini, Enea, Taverni, Gemma,  
555 Payvand, Melika, & Donati, Elisa. (2020). EMG and Video Dataset for sensor fusion based hand  
556 gestures recognition (Version 3.0). All the code used for the reported experiments can be found at  
557 [https://github.com/Enny1991/dvs\\_emg\\_fusion](https://github.com/Enny1991/dvs_emg_fusion)

## REFERENCES

- 558 Amir, A., Taba, B., Berg, D., Melano, T., McKinstry, J., Nolfo, C. D., et al. (2017). A low power, fully  
559 event-based gesture recognition system. In *2017 IEEE Conference on Computer Vision and Pattern  
560 Recognition (CVPR)*. 7388–7397. doi:10.1109/CVPR.2017.781
- 561 Anumula, J., Neil, D., Delbruck, T., and Liu, S.-C. (2018). Feature representations for neuromorphic audio  
562 spike streams. *Frontiers in neuroscience* 12, 23
- 563 Atzori, M., Gijssberts, A., Castellini, C., Caputo, B., Hager, A.-G. M., Elsig, S., et al. (2014).  
564 Electromyography data for non-invasive naturally-controlled robotic hand prostheses. *Scientific data* 1,  
565 140053
- 566 Barker, J., Marxer, R., Vincent, E., and Watanabe, S. (2015). The third ‘chime’ speech separation  
567 and recognition challenge: Dataset, task and baselines. *2015 IEEE Workshop on Automatic Speech  
568 Recognition and Understanding (ASRU)*, 504–511

- 569 Benatti, S., Casamassima, F., Milosevic, B., Farella, E., Schönle, P., Fateh, S., et al. (2015). A versatile  
570 embedded platform for emg acquisition and gesture recognition. *IEEE transactions on biomedical*  
571 *circuits and systems* 9, 620–630
- 572 Benjamin, B. V., Gao, P., McQuinn, E., Choudhary, S., Chandrasekaran, A. R., Bussat, J.-M., et al. (2014).  
573 Neurogrid: A mixed-analog-digital multichip system for large-scale neural simulations. *Proceedings of*  
574 *the IEEE* 102, 699–716
- 575 Biagetti, G., Crippa, P., and Falaschetti, L. (2018). Classifier level fusion of accelerometer and semg  
576 signals for automatic fitness activity diarization. *Sensors* 18, 2850. doi:10.3390/s18092850
- 577 Brader, J. M., Senn, W., and Fusi, S. (2007). Learning real-world stimuli in a neural network with  
578 spike-driven synaptic dynamics. *Neural computation* 19, 2881–2912
- 579 Braun, S., Neil, D., Anumula, J., Ceolini, E., and Liu, S. (2019). Attention-driven multi-sensor selection.  
580 In *2019 International Joint Conference on Neural Networks (IJCNN)*. 1–8. doi:10.1109/IJCNN.2019.  
581 8852396
- 582 Castanedo, F. (2013). A review of data fusion techniques. *TheScientificWorldJournal* 2013, 704504.  
583 doi:10.1155/2013/704504
- 584 Ceolini, E., Taverni, G., Khacef, L., Payvand, M., and Donati, E. (2019). Live demonstration: Sensor fusion  
585 using emg and vision for hand gesture classification in mobile applications. In *2019 IEEE Biomedical*  
586 *Circuits and Systems Conference (BioCAS)*. 1–1. doi:10.1109/BIOCAS.2019.8919163
- 587 Ceolini, E., Taverni, G., Khacef, L., Payvand, M., and Donati, E. (2019a). Sensor fusion using emg and  
588 vision for hand gesture classification in mobile applications. *arXiv preprint arXiv:1910.11126*
- 589 [Dataset] Ceolini, E., Taverni, G., Payvand, M., and Donati, E. (2019b). EMG and Video Dataset for sensor  
590 fusion based hand gestures recognition. doi:10.5281/zenodo.3228846
- 591 Chan, V., Liu, S.-C., and van Schaik, A. (2007). Aer ear: A matched silicon cochlea pair with address event  
592 representation interface. *IEEE Transactions on Circuits and Systems I: Regular Papers* 54, 48–59
- 593 Chen, C., Yu, Y., Ma, S., Sheng, X., Lin, C., Farina, D., et al. (2020). Hand gesture recognition based on  
594 motor unit spike trains decoded from high-density electromyography. *Biomedical Signal Processing and*  
595 *Control* 55, 101637
- 596 Cheok, M. J., Omar, Z., and Jaward, M. H. (2019). A review of hand gesture and sign language recognition  
597 techniques. *International Journal of Machine Learning and Cybernetics* 10, 131–153
- 598 Cholet, S., Paugam-Moisy, H., and Regis, S. (2019). Bidirectional associative memory for multimodal  
599 fusion : a depression evaluation case study. In *2019 International Joint Conference on Neural Networks*  
600 *(IJCNN)*. 1–6. doi:10.1109/IJCNN.2019.8852089
- 601 Cicirelli, G., Attolico, C., Guaragnella, C., and D’Orazio, T. (2015). A kinect-based gesture recognition  
602 approach for a natural human robot interface. *International Journal of Advanced Robotic Systems* 12, 22



- 603 Corradi, F. and Indiveri, G. (2015). A neuromorphic event-based neural recording system for smart  
604 brain-machine-interfaces. *IEEE transactions on biomedical circuits and systems* 9, 699–709
- 605 Courbariaux, M., Bengio, Y., and David, J.-P. (2015). Binaryconnect: Training deep neural networks with  
606 binary weights during propagations. In *Advances in neural information processing systems*. 3123–3131
- 607 Davies, M. (2019). Benchmarks for progress in neuromorphic computing. *Nature Machine Intelligence* 1,  
608 386–388
- 609 Davies, M., Srinivasa, N., Lin, T.-H., Chinya, G., Cao, Y., Choday, S. H., et al. (2018). Loihi: A  
610 neuromorphic manycore processor with on-chip learning. *IEEE Micro* 38, 82–99
- 611 Debes, C., Merentitis, A., Heremans, R., Hahn, J., Frangiadakis, N., van Kasteren, T., et al. (2014).  
612 Hyperspectral and lidar data fusion: Outcome of the 2013 grss data fusion contest. *IEEE Journal of*  
613 *Selected Topics in Applied Earth Observations and Remote Sensing* 7. doi:10.1109/JSTARS.2014.  
614 2305441
- 615 Deiss, S. R., Douglas, R. J., Whatley, A. M., et al. (1999). A pulse-coded communications infrastructure  
616 for neuromorphic systems. *Pulsed neural networks* , 157–178
- 617 Deng, J., Dong, W., Socher, R., Li, L.-J., Li, K., and Fei-Fei, L. (2009). Imagenet: A large-scale hierarchical  
618 image database. In *2009 IEEE conference on computer vision and pattern recognition (Ieee)*, 248–255
- 619 Donati, E., Payvand, M., Risi, N., Krause, R., Burelo, K., Indiveri, G., et al. (2018). Processing emg signals  
620 using reservoir computing on an event-based neuromorphic system. In *2018 IEEE Biomedical Circuits*  
621 *and Systems Conference (BioCAS) (IEEE)*, 1–4
- 622 Donati, E., Payvand, M., Risi, N., Krause, R. B., and Indiveri, G. (2019). Discrimination of emg signals  
623 using a neuromorphic implementation of a spiking neural network. *IEEE transactions on biomedical*  
624 *circuits and systems*
- 625 Došen, S., Cipriani, C., Kostić, M., Controzzi, M., Carrozza, M. C., and Popović, D. B. (2010).  
626 Cognitive vision system for control of dexterous prosthetic hands: experimental evaluation. *Journal of*  
627 *neuroengineering and rehabilitation* 7, 42
- 628 Droniou, A., Ivaldi, S., and Sigaud, O. (2015). Deep unsupervised network for multimodal perception,  
629 representation and classification. *Robotics and Autonomous Systems* 71, 83 – 98. doi:https://doi.org/10.  
630 1016/j.robot.2014.11.005. Emerging Spatial Competences: From Machine Perception to Sensorimotor  
631 Intelligence
- 632 Edelman, G. M. (1987). *Neural Darwinism: The theory of neuronal group selection* (New York, US: Basic  
633 Books)
- 634 Frenkel, C., Lefebvre, M., Legat, J.-D., and Bol, D. (2019a). A 0.086-mm<sup>2</sup> 12.7-pj/sop 64k-synapse  
635 256-neuron online-learning digital spiking neuromorphic processor in 28-nm cmos. *IEEE Transactions*  
636 *on Biomedical Circuits and Systems* 13, 145–158

- 637 Frenkel, C., Legat, J.-D., and Bol, D. (2019b). Morp hic: A 65-nm 738k-synapse/mm<sup>2</sup> quad-core binary-  
638 weight digital neuromorphic processor with stochastic spike-driven online learning. *IEEE Transactions*  
639 *on Biomedical Circuits and Systems* 13, 999–1010
- 640 Furber, S. B., Galluppi, F., Temple, S., and Plana, L. A. (2014). The spinnaker project. *Proceedings of the*  
641 *IEEE* 102, 652–665
- 642 Gerstner, W. (1995). Time structure of the activity in neural network models. *Phys. Rev. E* 51, 738–758.  
643 doi:10.1103/PhysRevE.51.738
- 644 Ghazaei, G., Alameer, A., Degenaar, P., Morgan, G., and Nazarpour, K. (2017). Deep learning-based  
645 artificial vision for grasp classification in myoelectric hands. *Journal of neural engineering* 14, 036025
- 646 Gigli, A., Gregori, V., Cognolato, M., Atzori, M., and Gijssberts, A. (2018). Visual cues to improve  
647 myoelectric control of upper limb prostheses. In *2018 7th IEEE International Conference on Biomedical*  
648 *Robotics and Biomechatronics (Biorob)* (IEEE), 783–788
- 649 Guo, H., Chen, L., Shen, Y., and Chen, G. (2014). Activity recognition exploiting classifier level fusion  
650 of acceleration and physiological signals. *UbiComp 2014 - Adjunct Proceedings of the 2014 ACM*  
651 *International Joint Conference on Pervasive and Ubiquitous Computing* , 63–66doi:10.1145/2638728.  
652 2638777
- 653 Haria, A., Subramanian, A., Asokkumar, N., Poddar, S., and Nayak, J. S. (2017). Hand gesture recognition  
654 for human computer interaction. *Procedia computer science* 115, 367–374
- 655 Hoeks, C., Barentsz, J., Hambrock, T., Yakar, D., Somford, D., Heijmink, S., et al. (2011). Prostate  
656 cancer: Multiparametric mr imaging for detection, localization, and staging. *Radiology* 261, 46–66.  
657 doi:10.1148/radiol.11091822
- 658 Horwitz, B. and Poeppel, D. (2002). How can eeg/meg and fmri/pet data be combined? *Human brain*  
659 *mapping* 17, 1–3. doi:10.1002/hbm.10057
- 660 Hubara, I., Courbariaux, M., Soudry, D., El-Yaniv, R., and Bengio, Y. (2016). Binarized neural networks.  
661 In *Advances in neural information processing systems*. 4107–4115
- 662 Hubara, I., Courbariaux, M., Soudry, D., El-Yaniv, R., and Bengio, Y. (2017). Quantized neural networks:  
663 Training neural networks with low precision weights and activations. *The Journal of Machine Learning*  
664 *Research* 18, 6869–6898
- 665 Izhikevich, E. M. (2004). Which model to use for cortical spiking neurons? *IEEE Transactions on Neural*  
666 *Networks* 15, 1063–1070
- 667 Jiang, N., Dosen, S., Muller, K.-R., and Farina, D. (2012). Myoelectric control of artificial limbs—is there  
668 a need to change focus?[in the spotlight]. *IEEE Signal Processing Magazine* 29, 152–150
- 669 Lahat, D., Adali, T., and Jutten, C. (2015). Multimodal data fusion: An overview of methods, challenges,  
670 and prospects. *Proceedings of the IEEE* 103, 1449–1477. doi:10.1109/JPROC.2015.2460697

- 671 Lee, H.-Y., Hsu, C.-M., Huang, S.-C., Shih, Y.-W., and Luo, C.-H. (2005). Designing low power of  
672 sigma delta modulator for biomedical application. *Biomedical Engineering: Applications, Basis and*  
673 *Communications* 17, 181–185
- 674 Lichtsteiner, P., Posch, C., and Delbruck, T. (2006). A 128 x 128 120db 30mw asynchronous vision  
675 sensor that responds to relative intensity change. In *2006 IEEE International Solid State Circuits*  
676 *Conference-Digest of Technical Papers (IEEE)*, 2060–2069
- 677 Liu, H. and Wang, L. (2018). Gesture recognition for human-robot collaboration: A review. *International*  
678 *Journal of Industrial Ergonomics* 68, 355–367
- 679 Liu, S.-C., Delbruck, T., Indiveri, G., Whatley, A., and Douglas, R. (2014). *Event-based neuromorphic*  
680 *systems* (John Wiley & Sons)
- 681 Loss, J. F., Cantergi, D., Krumholz, F. M., La Torre, M., and Candotti, C. T. (2012). Evaluating the  
682 electromyographical signal during symmetrical load lifting. *Applications of EMG in Clinical and Sports*  
683 *Medicine* , 1
- 684 Markovic, M., Dosen, S., Cipriani, C., Popovic, D., and Farina, D. (2014). Stereovision and augmented  
685 reality for closed-loop control of grasping in hand prostheses. *Journal of neural engineering* 11, 046001
- 686 Markovic, M., Dosen, S., Popovic, D., Graimann, B., and Farina, D. (2015). Sensor fusion and computer  
687 vision for context-aware control of a multi degree-of-freedom prosthesis. *Journal of neural engineering*  
688 12, 066022
- 689 Meier, K. (2015). A mixed-signal universal neuromorphic computing system. In *2015 IEEE International*  
690 *Electron Devices Meeting (IEDM) (IEEE)*, 4–6
- 691 Merolla, P. A., Arthur, J. V., Alvarez-Icaza, R., Cassidy, A. S., Sawada, J., Akopyan, F., et al. (2014). A  
692 million spiking-neuron integrated circuit with a scalable communication network and interface. *Science*  
693 345, 668–673
- 694 Moons, B., Goetschalckx, K., Van Berckelaer, N., and Verhelst, M. (2017). Minimum energy quantized  
695 neural networks. In *2017 51st Asilomar Conference on Signals, Systems, and Computers (IEEE)*,  
696 1921–1925
- 697 Moradi, S., Qiao, N., Stefanini, F., and Indiveri, G. (2017). A scalable multicore architecture with  
698 heterogeneous memory structures for dynamic neuromorphic asynchronous processors (dynaps). *IEEE*  
699 *transactions on biomedical circuits and systems* 12, 106–122
- 700 Neckar, A., Fok, S., Benjamin, B. V., Stewart, T. C., Oza, N. N., Voelker, A. R., et al. (2018).  
701 Braindrop: A mixed-signal neuromorphic architecture with a dynamical systems-based programming  
702 model. *Proceedings of the IEEE* 107, 144–164
- 703 Neftci, E., Mostafa, H., and Zenke, F. (2019). Surrogate gradient learning in spiking neural networks.  
704 *ArXiv abs/1901.09948*

- 705 Orchard, G., Jayawant, A., Cohen, G. K., and Thakor, N. (2015). Converting static image datasets to  
706 spiking neuromorphic datasets using saccades. *Frontiers in neuroscience* 9, 437
- 707 Paszke, A., Gross, S., Chintala, S., Chanan, G., Yang, E., DeVito, Z., et al. (2017). Automatic differentiation  
708 in PyTorch. *NeurIPS Autodiff Workshop*
- 709 Peng, L., Chen, L., Wu, X., Guo, H., and Chen, G. (2016). Hierarchical complex activity representation and  
710 recognition using topic model and classifier level fusion. *IEEE Transactions on Biomedical Engineering*  
711 64, 1369–1379
- 712 Phinyomark, A., N Khushaba, R., and Scheme, E. (2018). Feature extraction and selection for myoelectric  
713 control based on wearable emg sensors. *Sensors* 18, 1615
- 714 Pitti, A., Blanchard, A., Cardinaux, M., and Gaussier, P. (2012). Gain-field modulation mechanism  
715 in multimodal networks for spatial perception. In *2012 12th IEEE-RAS International Conference on*  
716 *Humanoid Robots (Humanoids 2012)*. 297–302. doi:10.1109/HUMANOIDS.2012.6651535
- 717 Qiao, N., Mostafa, H., Corradi, F., Osswald, M., Stefanini, F., Sumislawska, D., et al. (2015). A  
718 reconfigurable on-line learning spiking neuromorphic processor comprising 256 neurons and 128k  
719 synapses. *Frontiers in neuroscience* 9, 141
- 720 Rivet, B., Wang, W., Naqvi, S. M., and Chambers, J. A. (2014). Audiovisual speech source separation: An  
721 overview of key methodologies. *IEEE Signal Processing Magazine* 31, 125–134. doi:10.1109/MSP.  
722 2013.2296173
- 723 Rueckauer, B., Lungu, I.-A., Hu, Y., Pfeiffer, M., and Liu, S.-C. (2017). Conversion of continuous-valued  
724 deep networks to efficient event-driven networks for image classification. *Frontiers in neuroscience* 11,  
725 682
- 726 Shivappa, S. T., Trivedi, M. M., and Rao, B. D. (2010). Audiovisual information fusion in human–computer  
727 interfaces and intelligent environments: A survey. *Proceedings of the IEEE* 98, 1692–1715. doi:10.1109/  
728 JPROC.2010.2057231
- 729 Shrestha, S. B. and Orchard, G. (2018). SLAYER: Spike layer error reassignment in time. In *Advances in*  
730 *Neural Information Processing Systems 31*, eds. S. Bengio, H. Wallach, H. Larochelle, K. Grauman,  
731 N. Cesa-Bianchi, and R. Garnett (Curran Associates, Inc.), 1419–1428
- 732 Smith, L. and Gasser, M. (2005). The development of embodied cognition: Six lessons from babies.  
733 *Artificial Life* 11, 13–29. doi:10.1162/1064546053278973
- 734 Smith, L. H., Hargrove, L. J., Lock, B. A., and Kuiken, T. A. (2011). Determining the optimal window  
735 length for pattern recognition-based myoelectric control: Balancing the competing effects of classification  
736 error and controller delay. *IEEE Transactions on Neural Systems and Rehabilitation Engineering* 19,  
737 186–192. doi:10.1109/TNSRE.2010.2100828

- 738 Tan, A.-H., Subagdja, B., Wang, D., and Meng, L. (2019). Self-organizing neural networks for universal  
739 learning and multimodal memory encoding. *Neural Networks* doi:[https://doi.org/10.1016/j.neunet.2019.](https://doi.org/10.1016/j.neunet.2019.08.020)  
740 08.020
- 741 Thakur, C. S., Molin, J. L., Cauwenberghs, G., Indiveri, G., Kumar, K., Qiao, N., et al. (2018). Large-scale  
742 neuromorphic spiking array processors: A quest to mimic the brain. *Frontiers in neuroscience* 12, 891
- 743 Turk, M. (2014). Multimodal interaction: A review. *Pattern Recognition Letters* 36, 189 – 195. doi:<https://doi.org/10.1016/j.patrec.2013.07.003>
- 744
- 745 Yasen, M. and Jusoh, S. (2019). A systematic review on hand gesture recognition techniques, challenges  
746 and applications. *PeerJ Computer Science* 5, e218
- 747 Zahra, O. and Navarro-Alarcon, D. (2019). A self-organizing network with varying density structure  
748 for characterizing sensorimotor transformations in robotic systems. In *Towards Autonomous Robotic*  
749 *Systems*, eds. K. Althoefer, J. Konstantinova, and K. Zhang (Cham: Springer International Publishing),  
750 167–178
- 751 Zenke, F. and Ganguli, S. (2018). SuperSpike: Supervised Learning in Multilayer Spiking Neural Networks.  
752 *Neural Computation* 30, 1514–1541. doi:10.1162/neco\_a\_01086
- 753 Zhang, Y., Wang, Z., and Du, J. (2019). Deep fusion: An attention guided factorized bilinear pooling for  
754 audio-video emotion recognition. In *2019 International Joint Conference on Neural Networks (IJCNN)*.  
755 1–8. doi:10.1109/IJCNN.2019.8851942
- 756 Zhao, D. and Zeng, Y. (2019). Dynamic fusion of convolutional features based on spatial and temporal  
757 attention for visual tracking. In *2019 International Joint Conference on Neural Networks (IJCNN)*. 1–8.  
758 doi:10.1109/IJCNN.2019.8852301

## FIGURE CAPTIONS

**Table 1.** Comparison of traditional and neuromorphic systems on the task of gesture recognition for both single sensor and sensor fusion. The results of the accuracy are reported with mean and standard deviation obtained over a 3-fold cross validation.

System	Modality	Accuracy (%)	Energy (uJ)	Inference time (ms)	EDP (uJ * s)
<b>Spiking CNN</b> (Loihi)	EMG	55.7 ± 2.7	173.2 ± 21.2	5.89 ± 0.18	1.0 ± 0.1
	DVS	92.1 ± 1.2	815.3 ± 115.9	6.64 ± 0.14	5.4 ± 0.8
	EMG+DVS	96.0 ± 0.4	1104.5 ± 58.8	7.75 ± 0.07	8.6 ± 0.5
<b>CNN</b> (GPU)	EMG	68.1 ± 2.8	(25.5 ± 8.4) · 10 <sup>3</sup>	3.8 ± 0.1	97.3 ± 4.4
	APS	92.4 ± 1.6	(31.7 ± 7.4) · 10 <sup>3</sup>	5.9 ± 0.1	186.9 ± 3.9
	EMG+APS	95.4 ± 1.7	(32.1 ± 7.9) · 10 <sup>3</sup>	6.9 ± 0.05	221.1 ± 4.1
<b>Spiking MLP</b> (ODIN+MorphIC)	EMG	53.6 ± 1.4	7.42 ± 0.11	23.5 ± 0.35	0.17 ± 0.01
	DVS	85.1 ± 4.1	57.2 ± 6.8	17.3 ± 2.0	1.00 ± 0.24
	EMG+DVS	89.4 ± 3.0	37.4 ± 4.2	19.5 ± 0.3	0.42 ± 0.08
<b>MLP</b> (GPU)	EMG	67.2 ± 3.6	(23.9 ± 5.6) · 10 <sup>3</sup>	2.8 ± 0.08	67.2 ± 2.9
	APS	84.2 ± 4.3	(30.2 ± 7.5) · 10 <sup>3</sup>	6.9 ± 0.1	211.3 ± 6.1
	EMG+APS	88.1 ± 4.1	(32.0 ± 8.9) · 10 <sup>3</sup>	7.9 ± 0.05	253.0 ± 3.9

**Table 2.** Inference statistics of Loihi models on 200 ms-long samples.

Network	Accuracy %	Core Utilization	Dynamic Power (mW)	Inference Speedup
EMG-Loihi	55.74 ± 2.74	6	29.4 ± 3.6	(34.01 ± 1.01) ×
DVS-Loihi	92.14 ± 1.23	95	109.0 ± 15.5	(30.14 ± 0.65) ×
Fusion-Loihi	96.04 ± 0.48	100	137.2 ± 7.3	(25.82 ± 0.24) ×

**Table 3.** Inference statistics of ODIN and MorphIC models on 200 ms-long samples.

Network	Accuracy (%)	Chip utilization (%)		Dyn. power (mW)		Processing time (ms)		Inference speedup
		ODIN	MorphIC	ODIN	MorphIC	ODIN	MorphIC	
EMG-ODIN	53.65 ± 1.37	91.8	–	0.315	–	23.5	–	8.5 ×
DVS-MorphIC	85.17 ± 4.11	–	42.0	–	3.3	–	17.3	11.6 ×
Fusion-ODIN	89.44 ± 3.02	91.8	41.0	0.315	3.3	19.5	9.5	10.3 ×

**Table 4.** Low-power operating conditions of ODIN and MorphIC at minimum supply voltage.

Chip	Supply voltage	$E_{SOP}$	Max. $f_{clk}$
ODIN	0.55V	8.4pJ	75MHz
MorphIC	0.8V	30pJ	55MHz



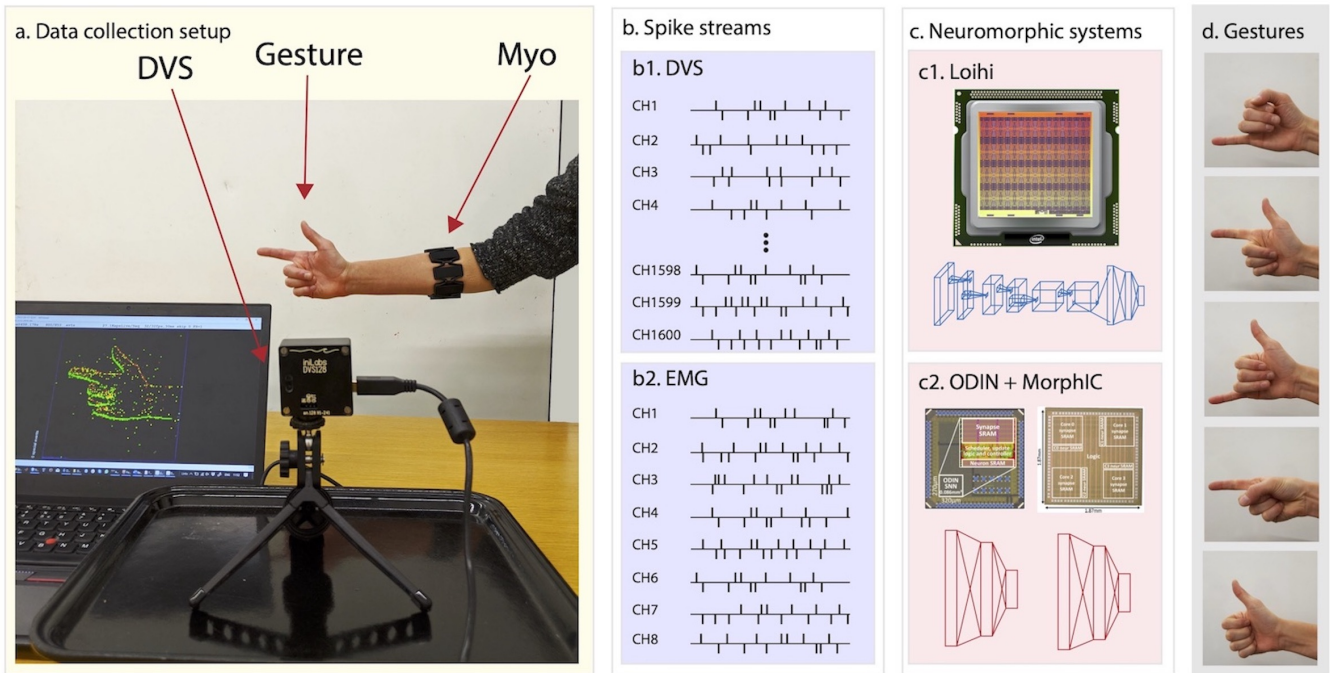


**Figure 1.** System overview. From left to right: (a) data collection setup featuring the DVS, the traditional camera and the subject wearing the EMG armband sensor, data streams of (b1) DVS and (b2) EMG transformed into spikes via the Sigma Delta modulation approach, the two neuromorphic systems namely (c1) Loihi and (c2) ODIN + MorphIC, (d) the hand gestures that the system is able to recognize in real time.

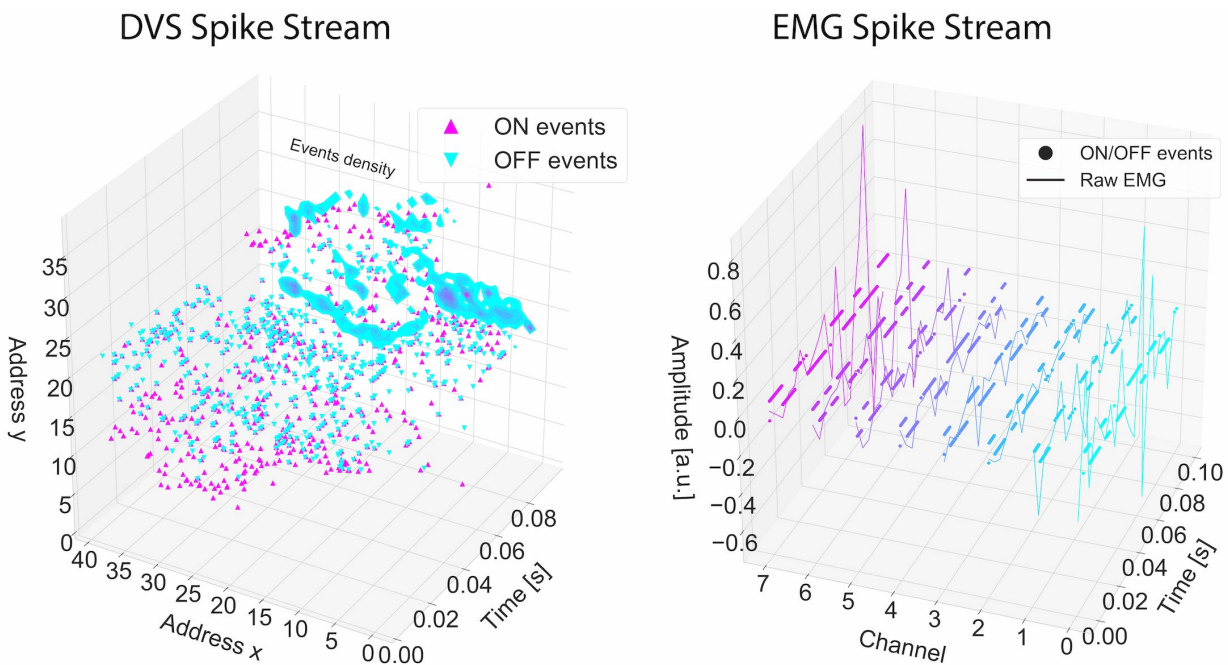


**Figure 2.** Example, for a gesture ‘elle’, of spike streams for DVS (left) and EMG (right). In the EMG figure the spikes are represented by dots while the continuous line is the raw EMG. Different channels have different colors.

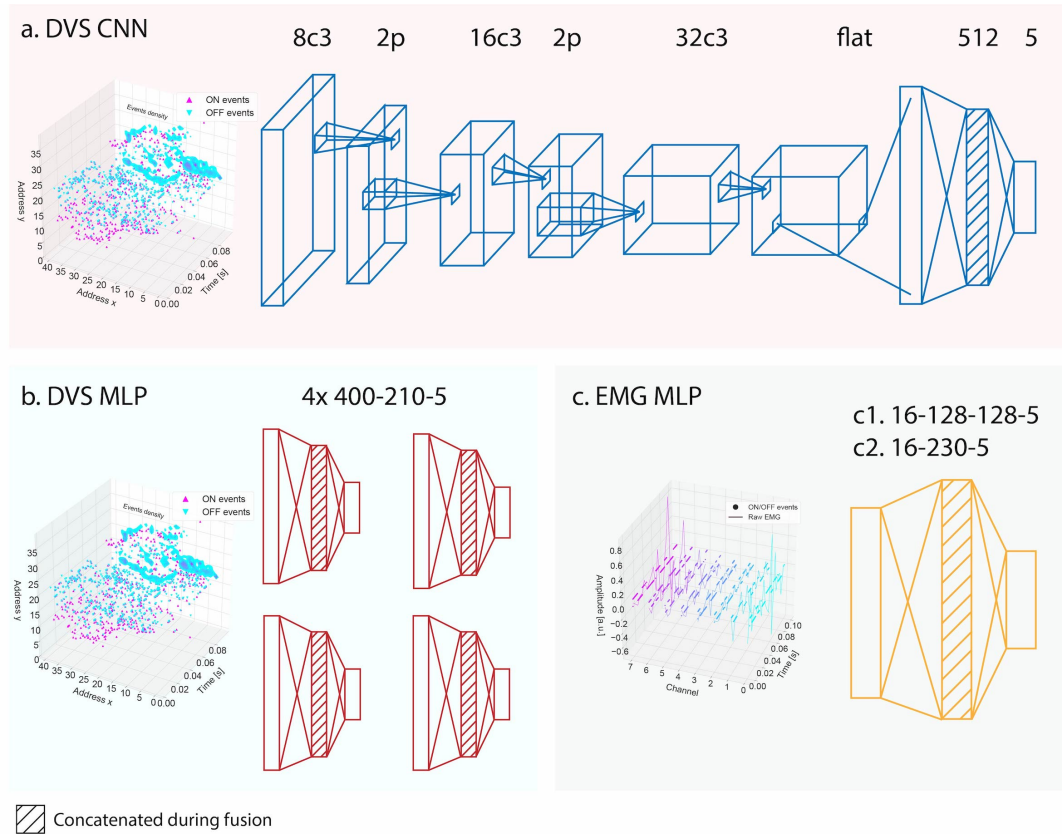


**Figure 3.** Architectures of the neural networks implemented on the neuromorphic systems and used in the baselines. (a) CNN architecture implemented on Loihi, the corresponding baseline CNN receives APS frames instead of DVS events. (b) subMLP architectures implemented on MorphIC, the corresponding baseline subMLPs receive APS frames instead of DVS events. (c) MLP architecture for the EMG data implemented on Loihi (c1) and on ODIN (c2), the corresponding baseline MLPs receive EMG features instead of EMG events. The shading indicates those layers that are concatenated during the fusion of the networks.

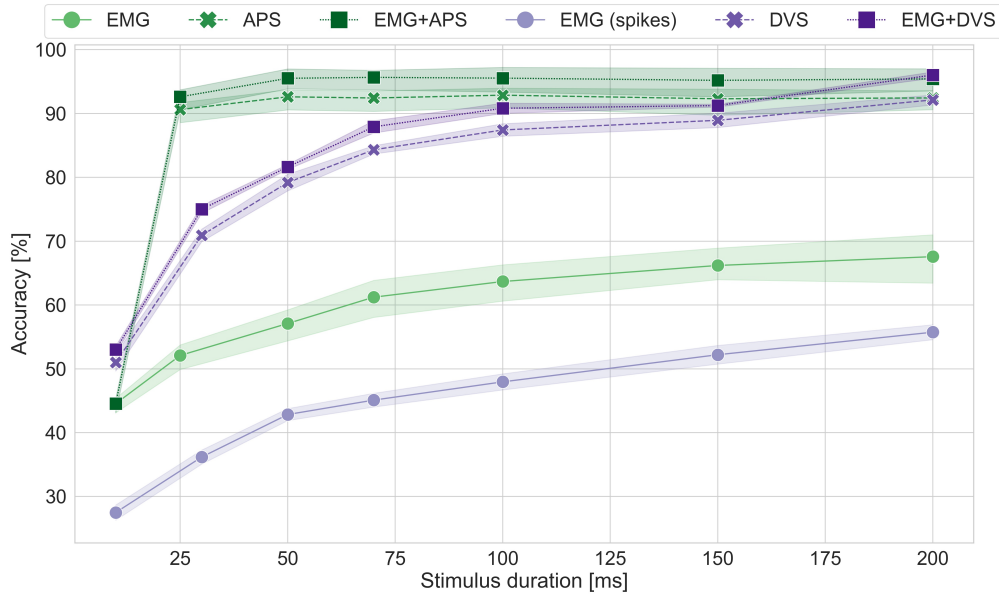


**Figure 4.** Accuracy vs stimulus duration for the Loihi system and its software baseline counterpart. In green the results for the CNN (GPU), in purple the results for the spiking CNN (Loihi). No classification is present for APS frames before 50 ms since the frame rate is 20 fps.

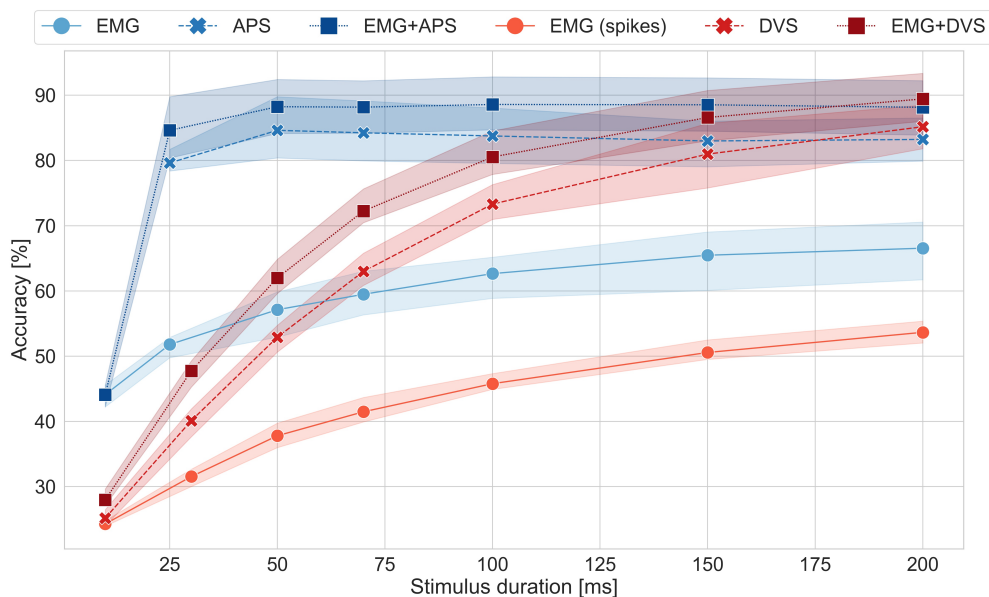


**Figure 5.** Accuracy vs stimulus duration for the ODIN + MorphIC system and its software baseline counterpart. In blue the results for the MLP (GPU), in red the results for the spiking MLP (ODIN+MorphIC). No classification is present for APS frames before 50 ms since the frame rate is 20 fps.

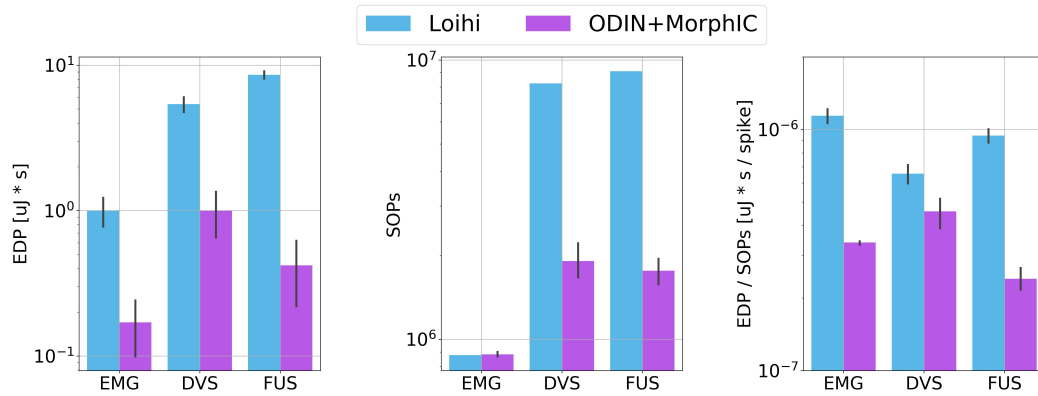


**Figure 6.** Comparison between the two neuromorphic system with respect to (a) energy delay product (EDP) (see Section 1), (b) number of synaptic operations (SOPs) (see Section 2.3.1), (c) EDP normalized by the number of SOPs.